Indian Geotech J (December 2018) 48(4):595–614
https://doi.org/10.1007/s40098-018-0338-y

ORIGINAL PAPER

Realistic Parameters Adoption to Solve Rock Engineering Problems

T. Ramamurthy[1]

Received: 28 August 2018 / Accepted: 24 October 2018 / Published online: 4 December 2018

Abstract Strength and modulus of rock mass as obtained from RMR, Q and GSI have been examined with reference to modulus ratio, M_{rj}, for their reliability. The design parameters adopted in some case studies based on these rock mass classifications are presented. The modulus ratios in these case studies are found to be much higher than those of the corresponding values of intact rocks, even after back analyses. Based on joint factor, J_f, compressive strength, modulus, cohesion and friction angle were estimated and applied in the analyses of a few cases. The predictions of deformations agreed well with the field measurements. Based on extensive experimental data of jointed specimens of rock and rock-like materials, a joint factor, J_f, was defined as a weakness coefficient in rock mass compared to the corresponding intact rock. J_f is linked to the strength, modulus and modulus ratio of rock mass. The modulus ratio, M_{rj}, of rocks is less than the modulus ratio of intact rock. The M_{rj} concept has been adopted to present a unified classification for intact rocks and rocks masses, to define soil that rock boundary and penetration rate of TBMs.

Keywords Case studies · Classifications · Equivalent continuum model · Joint factor · Modulus ratio · Numerical modeling · Penetration rate of TBMs · Properties · Rock mass · Soil–rock boundary

✉ T. Ramamurthy
temuraramamurthy@yahoo.com

[1] Angron Geotech Pvt. Ltd, Naraina Industrial Area, Phase II, New Delhi 110028, India

Introduction

Soil and rock are geotechnical materials formed through very complex processes. Soil is treated most often as a continuum, i.e., homogeneous and isotropic, for the purpose of analysis and design, even though it is a particulate material. An undisturbed specimen can be obtained from the field, or a remolded specimen is prepared in the laboratory to the required density and water content and tested to assess the required soil parameters under relevant drainage conditions, confining pressures either in axisymmetrical or in asymmetrical stress states. A soil test specimen is so chosen that its minimum dimension is many times larger than the maximum soil particle size to get representative and consistent results.

It is not so in the case of rock masses. They are discontinuous, non-homogeneous, anisotropic and prestressed. Collection of undisturbed specimen of rock mass to test in a laboratory is considered uneconomical and mostly not practicable. In some cases, large field shear and plate load tests are conducted to assess rock mass properties. Even these tests are being considered time-consuming and expensive. So tests are conducted as a routine on intact rock specimens in a laboratory to arrive at the upper bound values of rock parameters. Attempts have been made to correlate strength and modulus of intact rock with those of rock mass through rock mass classifications. These correlations are often being adopted to assess compressive strength (σ_{cj}), modulus (E_j), cohesion (c_j), friction angle (ϕ_j) and to predict stress strain response of rock mass during the last four decades; subscript j refers to rock mass.

Hypothetical stress–strain curves for three different rocks are presented in Fig. 1. Curves OA, OB and OC represent three stress–strain curves with failure occurring at A, B and C, respectively. Curves OA and OB have same

modulus but different strengths and strains at failure, whereas the curves OA and OC have same strength but different moduli and failure strains. So neither strength nor modulus alone could be chosen to represent the overall quality of the rock. Therefore, strength and modulus together will give a realistic understanding of the rock response for engineering usage. This approach to define the quality of intact rocks was proposed by Deere and Miller [1] by considering the modulus ratio, $M_{ri} = E_i/\sigma_{ci}$, where E_i = tangent modulus at 50% of failure strength, σ_{ci} = compressive strength at failure, and i is subscript for intact rock.

Modulus Ratio Concept

Deere and Miller presented a classification of intact rocks based on modulus value (E_i) at 50% of the failure stress and the unconfined compressive strength (σ_{ci}). Vast experimental data of 613 rock specimens from different locations covering 176 igneous, 193 sedimentary, 167 metamorphic and 77 limestones and dolomites were presented by them to classify intact rocks on the basis of (σ_{ci}) and modulus ratio, $M_{ri}(= E_i/\sigma_{ci})$. It is found that for basalts and limestones, one could expect M_{ri} values up to 1600, whereas for shales this value could be close to 60. Even weathered Keuper showed M_{ri} close to 50. Only chalks with high porosity have shown M_{ri} greater than 1000 [2] due to high modulus and low strength.

Rock Mass Parameters from Classifications

The most commonly adopted rock mass classifications are RMR, Q and GSI systems at present. Significant contributions have come from Bieniawski [3] and Barton et al. [4] based on their vast experience in a number of tunnels. Erlier GSI classification by Hoek [5] and Hoek and Brown [6] was a combination of RMR and Q approaches with some modification. The value of GSI was same as RMR as suggested by Bieniawski [7] for RMR > 18 and, for GSI < 18, Q values were considered for the rock mass. Later on, they suggested to arrive at GSI based on fracture intensity and degree of joint roughness matching with sketches and table. Often designers adopt one or more classifications to arrive at conservative designs.

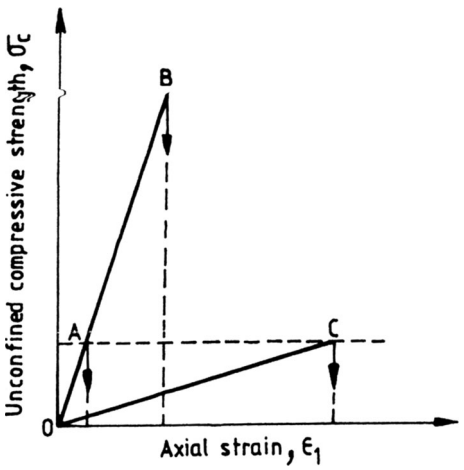

Fig. 1 Hypothetical stress–strain curves

Strength and Modulus from RMR

Bieniawski [3] suggested shear strength parameters, c_j (cohesion) and ϕ_j (friction angle), where subscript j refers to rock mass, for five levels of rock mass classes (Table 1). These parameters have been in use for over 4 decades. With these values of c_j and ϕ_j, the uniaxial compressive strengths (σ_{cj}) of the mass are calculated as per Mohr–Coulomb criterion, Eq. (1) and are referred in Table 2

$$\sigma_{cj} = 2c_j \cos\phi_j/(1 - \sin\phi_j). \quad (1)$$

Table 2 includes the estimated values of E_j from Eq. (2) as per Serafim and Pereira [8],

$$E_j = 10^{(RMR-10)/40}, \text{ GPa}. \quad (2)$$

It is obvious from this table that the modulus ratios, $M_{rj} = E_j/\sigma_{cj}$, decrease with the decrease in RMR, but the values are extremely high for rock masses, as compared to intact rocks [1].

Strength and Modulus from Q

Barton [9] suggested modification to the earlier Q values [4] by considering the influence of uniaxial compressive strength of the intact rock (σ_{ci}) in the following form

$$Q_c = Q\sigma_{ci}/100 \quad (3)$$

and recommended Q_c values for estimating the compressive strength and modulus of rock mass as

$$\sigma_{cj} = 5\gamma Q_c^{1/3}, \text{ MPa and} \quad (4)$$

$$E_j = 10\,Q_c^{1/3}, \text{ GPa}, \quad (5)$$

where γ density of rock mass in g/cc or t/m^3. Equation (4) suggests that Q is linked to the compressive strength of rock mass through the intact rock strength. On the contrary, the modulus of rock mass, E_j, is not linked to the modulus of the intact rock through Q.

Another important recommendation of Barton [9] is to assess c_j and ϕ_j of rock mass from the following expressions,

Table 1 RMR strength values for rock masses [3]

Rating	100–81	80–61	60–41	40–21	< 20
Cohesion, KPa	> 400	300–400	200–300	100–200	< 100
Friction angle	> 45°	35°–45°	25°–35°	15°–25°	< 15°

Table 2 M_{rj} values with RMR for rock masses

RMR	σ_{cj}, MPa	E_j, GPa	M_{rj} E_j/σ_{cj}
100	3.5[a]	177.80	50,800
80	1.97	56.20	28,528
60	1.18	17.80	15,085
40	0.64	5.60	8750
20	0.26	1.78	6846

[a]Value by extrapolation; E_j from Serafim and Pereira [8]

$$c_j = (\mathrm{RQD}/J_s)(1/\mathrm{SRF})\,(\sigma_{ci}/100),\ \mathrm{MPa} \quad (6)$$

$$\phi_j^\circ = \tan^{-1}(J_r J_w/J_a), \quad (7)$$

where J_s is joint set number (Barton uses J_n), SRF is the stress reduction number, J_r is joint roughness number, J_w is for seepage and its pressure, and J_a is joint alteration number.

With the data provided in Tables 6 and 7 of Barton [9], the values of compressive strength of rock mass are calculated as per Mohr–Coulomb criterion, Eq. (1) with c_j and ϕ_j, and are referred to as σ_{cj2} in Table 3 of this paper. The data in this table suggest that σ_{cj2} values differ significantly from the suggested values (σ_{cj1}) by Eq. (4). The ratio of $\sigma_{cj1}/\sigma_{cj2}$ varies from 1:7 to 54:1 depending upon the value of Q_c. This table also gives the values of E_j as per Barton [9]. The values of modulus ratio, M_{rj}, are more or less constant and are around 800; in fact, Eqs. (4, 5) give this ratio as 800 for a value of density, γ = 2.5 g/cc, irrespective of Q_c varying from 0.008 to 100, i.e., whether the rock is intact, jointed, isotropic or anisotropic.

Strength and Modulus from GSI

Hoek [5] and Hoek and Brown [6] advocate the adoption of Geological Strength Index, GSI, to estimate the material parameters, m_j and s_j, of the Hoek–Brown failure criterion to predict strength under any desired confining pressure. GSI was based on both RMR and Q systems with some modifications mainly to estimate the compressive strength of rock mass. Their original expression is Eq. (8).

$$\sigma_{cj}/\sigma_{ci} = \sqrt{s_j};\quad s_j = \exp[(\mathrm{GSI} - 100)/9]. \quad (8)$$

There have been modifications subsequently to estimate s_j and $\sqrt{s_j}$ by considering disturbance factor, D. For estimating the deformation modulus, Hoek [5] recommends the use of Eq. (2) using RMR as per Bieniawski [3] and not the GSI value.

The values of GSI, s_j and E_j given in Table 5 of Hoek [5] have been considered in calculating the values of modulus ratio, M_{rj}, in Table 4 of this paper. The values of M_{rj} are surprisingly high, ranging from 1500 to 1720 with an average value of 1621 for GSI varying from 85 to 34. These values of M_{rj} do not decrease, with the decrease in GSI value.

Parameters Used in Case Studies

The design parameters, i.e., compressive strength and modulus of rock mass (E_j), adopted in some of the recent projects based on rock mass classifications have been checked with M_r concept. Only those cases, in which the parameters of intact and rock mass are available, have shown that M_{rj} values are much higher than M_{ri}. This is contrary to the experimental evidence of jointed specimens. In the following, these cases are briefly presented.

1. In the underground pump storage development of Rio Grande No. 1, Argentina, massive gneiss Pelado was encountered [10]. The RQD of the rock mass varied from 65 to 90%. The modulus of intact rock, E_i varied from 30 to 60 GPa, and compression test gave σ_{ci} = 140 MPa. But the triaxial compression test gave σ_{ci} = 110 MPa with c_i = 20 MPa and $\phi_j = 50^\circ$. The M_{ri} would range from 273 to 546. The field shear test gave c_j = 0.34 MPa and $\phi_j = 30^\circ$ (peak) resulting in $\sigma_{cj} = 1.25$ MPa as per Mohr–Coulomb theory. The modulus of deformation, E_d, from plate loading test varied from 40 to 90 GPa from loading and unloading cycles; average being $E_d = 60$ GPa, adopted in

Table 3 Values of σ_{cj}, c_j, ϕ_j and E_j as per Barton [9] for σ_{ci} = 100 MPa, γ = 2.5 g/cc

Q_c	σ_{cj1} MPa	c_j MPa	ϕ_j° MPa	σ_{cj2} MPa	$\sigma_{cj1}/\sigma_{cj2}$	E_j GPa	M_{rj}
100	58.0	50	63	412.7	1/7	40	690
10	26.9	10	45	48.3	1/1.8	22	818
1.2	13.3	2.5	26	8.0	1.7	10.7	805
0.04	4.3	0.26	9	0.61	7.0	3.5	814
0.008	1.2	0.01	5	0.022	54	0.9	750
Before grouting							
0.40	9.0	1.7	14	4.4	2.05	7.0	778
After grouting							
8.3	25	8.3	63	69	1/2.6	20.0	800

σ_{cj1} from Barton, Eq. (4)

σ_{cj2} from c_j and ϕ_j values Eqs. (6, 7)

Table 4 Prediction of σ_{cj}, E_j and M_{rj} for σ_{ci} = 100 MPa. Data from Hoek [5]

GSI	s_j	σ_{cj}, MPa	E_j, GPa	$M_{rj} = E_j/\sigma_{cj}$
85	0.190	43.6	75	1720
75	0.062	24.9	40	1606
65	0.021	14.5	24	1655
62	0.015	12.2	20	1639
60	0.012	11.0	18	1636
50	0.004	6.3	10	1587
48	0.003	5.5	9	1636
40	0.0013	3.6[a]	6	1667
38	0.001	3.2	5	1563
34	0.0004	2.0	3	1500
			Average	1621

[a]Estimated from Eq. (8)

the analysis. Finite element (FE) and boundary element (BE) analyses were conducted with K_0 varying from 0.5 to 2.0, considering the rock as elastic medium. The M_{rj} = 4800 and M_{rj}/M_{ri} = 8.79 by considering the maximum M_{ri}. These values are rather very high; the M_{rj}/M_{ri} should have been less than 1.0. They have indicated that the measured deformations were only twice the calculated values.

2. The rock encountered in the Masua mine, Italy, was dolomite limestone with RMR = 80, σ_{ci} = 87.8 MPa, E_i = 78 GPa, σ_t = 5.6 MPa, c_i = 31 MPa, $\phi_i = 45^\circ$ and M_{ri} = 888, [11]. From the field plate loading test for the predominantly isotropic rock, E_d varied from 37.5 ± 5.5 GPa.. The final RMR chosen was 68 ± 10.8, and from GSI, σ_{cj} estimated was 15.8123 ± 0.0046 MPa. The E_j varied between 32 and 43 GPa with average being 37.5 GPa. The ratio M_{rj}/M_{ri} is, therefore, for maximum value of M_{rj}, 3.07 and for minimum is 2.28. By adopting discontinuity method for 3D analysis and FEM for 2D analysis, it has been mentioned that the deformations on the hanging wall of the southern open slope were of the same range of the predicted values.

3. Hoek and Moy [12] dealt with various aspects of "Power house caverns in weak rock." For siltstone, σ_{ci} = 100 MPa, RMR = 48, E_d = 8.9 GPa, s_j = 0.003 resulting σ_{cj} = 5.477 MPa; No E_i value is available. M_{rj} = 1625, appears to be rather high for RMR = 48. Even by assuming a high value of M_{ri} = 500, M_{rj}/M_{ri} = 3.25.

4. In their contribution on "Practical estimates of rock mass strength," Hoek and Brown [6] recommendations indicate

(a) For good quality rock (GSI = 75), σ_{cj} = 64.8 MPa, E_j = 42 GPa, M_{rj} = 648
(b) For Avrg. quality rock (GSI = 50), σ_{cj} = 13.0 MPa, E_j = 9.0 GPa, M_{rj} = 692
(c) For poor quality rock (GSI = 30), σ_{cj} = 1.7 MPa, E_j = 1.4 GPa, M_{rj} = 824

(d) For Braden braccia, El Teniete mine, Chile
GSI = 75, $c_j = 4.32$ MPa, $\phi_j = 42°$, $\sigma_{cj} = 19.4$ MPa, $E_j = 30$ GPa, M_{rj} = 1546

(e) For Nathpa Jhakri HE Project, India,
Quartz mica schist (GSI = 65), $c_j = 2.0$ MPa, $\phi_j = 40°$, $\sigma_{cj} = 8.2$ MPa, $E_j = 13$ GPa, M_{rj} = 1585

(f) Athens schist—decomposed, GSI = 20
$c_j = 0.09 - 0.018$ MPa, $\phi_j = 24°$, $\sigma_{cj} = 0.27 - 0.53$ MPa, $E_j = 398 - 562$ MPa
M_{rj} = 1060 (min) and 1474 (max.)

(g) Yacambu Quibor tunnel, Venezuela,
For poor quality graphitic phyllite, GSI = 24,
$c_j = 0.34$ MPa, $\phi_j = 24°$, $\sigma_{cj} = 1.0$ MPa, $E_j = 870$ MPa.

Note: M_{rj} values are rather high; stronger rocks having lower and weaker ones having higher values.

5. For the Mingtan Pump Storage Project, Taiwan, underground power cavern, 22 m wide, 46 m high, 158 m long, and a transformer hall, 13 m wide, 20 m high, 172 m long, are located at a depth of 300 m below the ground level in jointed sandstone and bedded sandstone [13].

1. For jointed sandstone, $\sigma_{ci} = 166$ MPa, $E_i = 22.3$ GPa, M_{ri} = 134
2. For bedded sandstone, $\sigma_{ci} = 66$ MPa, $E_i = 12.8$ GPa, M_{ri} = 194.

These are average values for rock cores.

The average RMR values for jointed sandstone and for bedded sandstone have been 69 and 58, respectively. They have adopted for:

1. Jointed sandstone: $\sigma_{cj} = 45 - 65$ MPa, $E_j = 29.85$ GPa, so M_{rj} = 543 and $M_{rj}/M_{ri} = 4.0$
2. Bedded sandstone: $\sigma_{cj} = 11.48$ MPa, $E_j = 15.85$ GPa, so M_{rj} = 1381 and $M_{rj}/M_{ri} = 7.1$.

When plate loading tests were conducted, the modulus of deformations (E_d) was much lower than the modulus as per Serafim and Pereira. For the jointed sandstone, E_d = 4.15 GPa and for bedded sandstone E_d = 2.9 GPa.

By adopting 2D finite difference programme FLAC, the progressive response of rocks was treated as elasto-plastic materials as per Mohr–Coulomb theory. Iterated analysis was carried out by lowering the parameters of rocks both intact and mass, to obtain deformations to match the measured ones. Finally, computed back analysis data were:

1. Jointed sandstone:
$\sigma_{ci} = 100$ MPa, $m_j = 4.298$, $s_j = 0.02047$ giving $\sigma_{cj} = 14.3$ MPa and $E_j = 4.5$ GPa, so $M_{rj} = 315$, $M_{rj}/M_{ri} = 2.4$.
2. For the bedded sandstone,
$\sigma_{ci} = 100$ MPa, $m_j = 1.519$, $s_j = 0.00211$ giving $\sigma_{cj} = 4.59$ MPa and $E_j = 2.5$ GPa,so $M_{rj} = 545$, $M_{rj}/M_{ri} = 2.8$.

In both the cases of sandstones, the M_{rj} values are higher than M_{ri} values even after conducting iterative analysis to match the measured deformations.

6. To provide appropriate support in the chromite mine, Ermekov et al. [14] carried out physical model studies by adopting equivalent material modeling with a scale of 1:50. For the horizontal working of chromite in the western Kazakhstan, they adopted three support systems: (i) framed arch, (ii) anchor supports with framed arch and (iii) injected anchored support with framed arch. The stress state at the depth of 135 m in the mine was estimated as σ_1 = 16 MPa, σ_2 = 14 MPa and σ_3 = 11 MPa.

The modulus of chromite cores, $E_i = 620$ GPa, $\sigma_{ci} = 31$ MPa, $M_{ri} = 2000$. For the rock cores surrounding the chromite, $\sigma_{ci} = 66$ MPa, $E_i = 46$ GPa, $M_{ri} = 697$. The σ_{cj} of chromite = 10 MPa, $E_j = 2.0$ GPa, $M_{rj} = 200$. For rock mass, $\sigma_{cj} = 20$ MPa, $E_j = 1.5$ GPa, $M_{rj} = 75$. Therefore, for chromite $M_{rj}/M_{ri} = 0.1$ and for the rock mass, $M_{rj}/M_{ri} = 0.11$. The properties chosen for chromite and rock mass not based on RMR, Q or GSI seem to be in order, i.e., M_{rj}/M_{ri} values are less than 1.0.

7. For the large span underground storage project, a cavern 25 m wide, 12 m high and 100 m long is located in Bukit Timah granite. Rock reinforcement was adopted as per Q-system and numerical modeling was also carried out [15]. Measurements and numerical analysis showed high horizontal stresses favouring the stability of the cavern. The crown showed upward deformation of the order of 1.0 mm only. σ_{ci} = 108–225 MPa (average 164 MPa, E_i = 49.3–113.3 GPa) (average 65.6 GPa). The estimated σ_{cj} = 45–65 MPa (average 55 MPa) and E_j = 40–50 GPa) (average 45 GPa). The $M_{ri} = 400$, $M_{rj} = 818$ and $M_{rj}/M_{ri} = 2.04$, which is more than 1.0.

8. For 1000 MW Masjed-e-Soloiman HEPP, Iran, Stabel and Samani [16] carried out 2D elasto-plastic hybrid FEM and BEM analyses on the powerhouse cavern, 30 m span, 50 m high and 151 m long located in mudstone consisting of layers of conglomerate, sandstone, siltstone and claystone. The rock core properties from laboratory tests of 1991 were:

1. Conglomerate:
$\sigma_{ci} = 57$ MPa, $E_i = 45$ GPa, so $M_{ri} = 789$
2. Sandstone: $\sigma_{ci} = 67$ MPa, $E_i = 25$ GPa, so $M_{ri} = 373$
3. Siltstone: $\sigma_{ci} = 39$ MPa, $E_i = 13$ GPa, so $M_{ri} = 333$
4. Claystone: $\sigma_{ci} = 23$ MPa, $E_i = 8$ GPa, so $M_{ri} = 348$.

In the analyses, the following properties of rock layers were chosen:

1. Conglomerate: $\phi_j = 43°$, $c_j = 2.87$ MPa, $\sigma_{cj} = 13.2$ MPa, $E_j = 15$ GPa, so, $M_{rj} = 1136$

2. Sandstone $\phi_j = 38^\circ$, $c_j = 1.67$ MPa, $\sigma_{cj} = 6.85$ MPa, $E_j = 7.0$ GPa, so,$M_{rj} = 1022$
3. Siltstone: $\phi_j = 30^\circ$, $c_j = 0.73$ MPa, $\sigma_{cj} = 2.53$ MPa, $E_j = 6.0$ GPa, so, $M_{rj} = 2372$
4. Claystone: $\phi_j = 24^\circ$, $c_j = 0.50$ MPa, $\sigma_{cj} = 1.54$ MPa, $E_j = 6.0$ GPa, so, $M_{rj} = 3896$

The σ_{cj} values are calculated from c_j and ϕ_j as per Mohr–Coulomb criterion. Therefore, for:

1. Conglomerate: $M_{rj}/M_{ri} = 1.44$
2. Sandstone: $M_{rj}/M_{ri} = 2.74$
3. Siltstone: $M_{rj}/M_{ri} = 7.12$
4. Claystone: $M_{rj}/M_{ri} = 11.20$.

These values are rather high.

9. Intake tunnel, Karuna III, HEPP, Iran: the analysis of the tunnel was carried out using 2D, UDEC and 3D elastic programmes [17]. Measured deformations agreed with the estimated values from back analysis. Back analysis was carried out using direct method UDEC software, and σ_{cj} and E_j were estimated. For Marly limestone/marl,

$c_j = 0.6$ MPa, $\phi_j = 30^\circ$, $\sigma_{cj} = 2.08$ MPa, $E_j = 6.0$ GPa.

By considering the average values of the rocks,

$\sigma_{ci} = 70$ MPa, $E_i = 10.25$ GPa, $M_{ri} = 146$ and $M_{rj} = 2855$, so, $M_{rj}/M_{ri} = 19.8$.

10. For the underground pumped powerhouse caverns, namely Samragjin, Muju, Sanchung, Yangyang and Chungsong, constructed during 1973–2003, the numerical softwares used were (1) visco-elastic FEM, (2) hybrid combining FEM and BEM and (3) elasto-plastic FEM [18]. The rock mass parameters were assumed by applying reduction factors to modulus (0.16–0.55) to cohesion (0.12–0.22), and to friction angle (0.6–0.87) to the corresponding values of intact rock cores. Mainly Mohr–Coulomb failure criterion was adopted. Detailed calculations with the parameters adopted for the analyses gave the following:

Rock type	Cavern	M_{rj}/M_{ri}	Convergence, mm
Granitic Gneiss	Muju	1.60	19.0
Porphyroblastic Gneiss	Sanchung	2.87	54.4
Porphyroblastic Gneiss, Granite Gneiss	Yangyang	3.83	55.0
Sandstone, Arkosic sandstone	Chungsong	3.30	50.0

For Samragjin cavern, reduction factors were not included in their paper

11. A synthetic rock mass (SRM) approach, which can take care of anisotropy and scale effects, was adopted by Carvalho et al. [19] to predict unconfined compressive and triaxial strengths. Clark [20], quoted by Lorig [21], using FLAC (ITASCA 2005) constructed SRM model based on actual scaled distribution of joints, and predicted strength in unconfined state with RMR covering anisotropy and scale effects as shown in Table 5. J_f and strength ratios (σ_{cj}/σ_{ci}) are also indicated. The SRM values agree reasonably well with the experimental findings based on joint factor, J_f.

12. Read [22], from synthetic rock mass (SRM) model for carbonatite 2D joints, gave

$\sigma_{ci} = 140$ MPa, $E_i = 60$ GPa, resulting $M_{ri} = 430$

1. For 20 m length of joint, $\sigma_{cj} = 80$ MPa, $E_j = 30$ GPa, $M_{rj} = 375$
2. For 40 m length of joint, $\sigma_{cj} = 60$ MPa, $E_j = 25$ GPa, $M_{rj} = 416$
3. For 80 m length of joint, $\sigma_{cj} = 70$ MPa, $E_j = 30$ GPa, $M_{rj} = 429$

Here, the M_{rj} values from 2D joint simulated rocks gave slightly lower values compared to the intact material. The SRM model seems to predict compressive strength and modulus values of simulated rock mass reasonably well in 2D case indicating negligible scale effect for the lengths of joints considered.

13. A stochastic analysis was carried out to estimate σ_{cj} and E_j of three grades of Ankara andesites by calculating the influence of correlations between relevant distributions on the simulated RMR values [23]. The model was also used in Monte Carlo simulation to estimate possible ranges of the Hoek–Brown strength parameters.

From minimum strength and modulus,

Table 5 Results of σ_{cj}/σ_{ci} from SRM and J_f [20]

RMR	σ_{cj}/σ_{ci} (SRM)	J_f^*	σ_{cj}/σ_{ci}
0	0.0	500	0.018
5	0.06	475	0.022
15	0.06	425	0.033
25	0.07	375	0.050
57	0.15	215	0.180
72	0.23	140	0.330
80	0.39	100	0.450
92	0.66	40	0.720
100	1.00	00	1.000

*J_f and RMR relation from RMR = 100 − (J_f/5) as per Ramamurthy [29]

Grade A : $M_{ri} = 520,\ M_{rj} = 7000;\ M_{rj}/M_{ri} = 13.46$

Grade B : $M_{ri} = 470,\ M_{rj} = 2113;\ M_{rj}/M_{ri} = 4.50$

Grade C : $M_{ri} = 359,\ M_{rj} = 1311;\ M_{rj}/M_{ri} = 3.65$

From maximum strength and modulus,

Grade A : $M_{ri} = 425,\ M_{rj} = 1568;\ M_{rj}/M_{ri} = 3.69$

Grade B : $M_{ri} = 431,\ M_{rj} = 1378;\ M_{rj}/M_{ri} = 3.20$

Grade C : $M_{ri} = 326,\ M_{rj} = 963;\ M_{rj}/M_{ri} = 2.95$

14. Waitaki dam block No. 10, New Zealand: A 3D FEM analysis was carried out for the Waitaki dam Richards and Read [24]. The tiltmeter deformations under the block No. 10 were matched to obtain in situ modulus E_j. The ratio E_j/E_i was 0.15 for GSI = 20 of class II Greywacke. This value (0.15) has been found to be very high, about 5 times, even for disturbance factor, $D = 0$ as per Hoek and Diederichs [25]. The intact rock properties were

$\sigma_{ci} = 50 - 60$ MPa, $E_i = 70$ GPa; $M_{rj} = 1167$ by considering $\sigma_{ci} = 60$ MPa.

As per Hoek and Brown [6] for GSI = 20,

$\sigma_{Cj} = 0.704$ MPa by considering $\sigma_{Ci} = 60$ MPa, $E_j = 10$ GPa, $M_{rj} = 14{,}205$, therefore $M_{rj}/M_{ri} = 12.2$.

15. Power house cavern, Rogun project, Kajikistan:

To predict deformations of roof and side walls using 3D FEM with M-C criterion, Bronshteyn et al. [26] adopted reduced c_i, ϕ_i and E_i as indicated here

For sandstone : $c = 3.0$ to 1.1 MPa(F.S. $= 2.7$),
$\phi^\circ = 50$ to 38(F.S. to $\tan\phi$: 1.53)
$E = 9000$ to 5000 MPa (F.S. $= 1.4$)
$M_{ri} = 546,\ M_{rj} = 1109;\ M_{rj}/M_{ri} = 2.03.$

For aleurolites : $c = 2$ to 0.5 MPa (F.S. $= 4.0$)
$\phi^\circ = 45$ to 32.5 (F.S. to $\tan\phi$: 1.56)
$E = 5500$ to 2670 (F.S. $= 2.06$)
$M_{ri} = 569,\ M_{rj} = 1467;\ M_{rj}/M_{ri} = 2.58.$

From a few case studies presented in the foregoing, it is obvious that strength and modulus adopted conclusively indicate M_{rj}/M_{ri} greater than 1.0.

Strength and Modulus from Join Factor J_f

Based on the extensive experimental results in uniaxial compression on jointed rocks and rock-like materials, the compressive strength of jointed mass is suggested close to the minimum values by Eq. (9) and the corresponding modulus by Eq. (10) [27],

$$\sigma_{cj}/\sigma_{ci} = \exp[-0.008\,J_f] \text{ and} \tag{9}$$

$$E_j/E_i = \exp[-0.0115\,J_f], \tag{10}$$

wherein J_f is a joint factor defined by Eq. (11)

$$J_f = J_n/n.r, \tag{11}$$

where J_n joint frequency, i.e, number of joints/meter, which takes care of RQD and joint sets and joint spacing; n inclination parameter depends on the inclination of sliding plane with respect to the major principal stress direction; the joint or set which is closer to $(45 - \phi_j/2)^\circ$ with the major principal stress will be the most critical one to experience sliding at first; r a parameter for joint strength; it takes care of the influence of closed or filled-up joint, thickness of gouge, roughness, extent of weathering of joint walls and cementation along the joint. This factor could be assessed in terms of an equivalent value of friction angle along the joint as $\tan\phi_j = \tau_j/\sigma_{nj}$ obtained from shear tests, in which τ_j is shear strength along the joint under an effective normal stress, σ_{nj}. The values of n and r are given in Tables 6, 7 and 8. When friction values are not available from shear tests, the same may be obtained from Table 8 based on intact rock strength. The variation of E_j/E_i with joint factor, J_f, is similar to the theoretical prediction by Walsh and Brace [28] and Hobbs [2] for one-dimensional compression between E_j/E_i versus joint frequency, J_n. But in Eq. (10), J_f involves not only J_n but also inclination of the critical joint and the strength likely to be mobilized along this joint.

Table 6 Values of n for different joint inclination, β° [27, 34]

β (°)	Type of anisotropy	
	U shaped	Shoulder shaped
0	0.82	0.85
10	0.46	0.60
20	0.11	0.20
30	0.05	0.06
40	0.09	0.12
50	0.30	0.45
60	0.46	0.80
70	0.64	0.90
80	0.82	0.95
90	0.95	0.98

Table 7 Suggested joint strength parameter, r, for filled-up joints at residual stage [27]

Gouge material	Friction angle ϕ_j, °	Joint strength, $r = \tan \phi_j$
Gravelly sand	45	1.00
Coarse sand	40	0.84
Fine sand	35	0.70
Silty sand	32	0.62
Clayey sand	30	0.58
Clayey silt		
Clay: 25%	25	0.47
Clay: 50%	15	0.27

Table 8 Suggested values of r for values of σ_{ci} [34]

Compressive strength, σ_{ci} (MPa)	Joint strength parameter, r	Remarks
2.5	0.30	Fine grained to coarse grained
5.0	0.45	
15.0	0.60	
25.0	0.70	
45.0	0.80	
65.0	0.90	
100.0	1.00	

Now from Eqs. (9) and (10), the modulus ratio of the jointed mass with respect to that of the intact rock is given by Eq. (12)

$$M_{rj}/M_{ri} = \exp[-0.0035 J_f] \quad (12)$$

Table 9 gives the estimated values of σ_{cj} and M_{rj} for different values of J_f varying from 0 to 500 for σ_{ci} = 100 MPa and M_{ri} = 500 of intact rock as an example. The M_{rj} values rapidly decrease with the increase in J_f. This table suggests that the relationship between E_j and σ_{cj} (i.e., M_{rj}) cannot be taken as constant or greater than M_{ri} when the rock mass experiences fracturing and undergoing change to lower quality.

Table 9 Estimation of σ_{cj} and M_{rj} from J_f for σ_{ci} = 100 MPa; assumed M_{ri} = 500 for intact rock

J_f	σ_{cj}, MPa	M_{rj}
0	100.00	500
100	44.90	352
200	20.20	248
300	9.10	175
400	4.10	123
500	1.80	87

M_{rj} from Eq. (12)

Classification Based on Strength and Modulus Ratio

Even though the original classification due to Deere and Miller was suggested only for intact rocks, by considering σ_{Ci} and E_i it was modified to classify rock masses as well [29]. It is a two-lettered classification: First letter suggests the range of σ_C and the second letter the range of M_r. The main advantage of such a classification (Tables 10 and 11) is that it not only takes into account two important engineering properties of the rock mass but also gives an assessment of the failure strain (ε_f) which the rock mass is likely to exhibit in the uniaxial compression, where in the stress–strain response it is nearly linear. That is,

$$\text{Modulus Ratio, } M_{rj} = E_{tj}/\sigma_{cj} = 1/\varepsilon_{fj}. \quad (13)$$

Further, the ratio of the failure strain of the jointed rock to that of the intact rock is given by

$$\varepsilon_{fi}/\varepsilon_{fj} = M_{rj}/M_{ri} = \exp\left(-3.50 \times 10^{-3} J_f\right). \quad (14)$$

On the basis of experimental data [27], the following simpler expression was also suggested,

$$\varepsilon_{fj} = 50\left(M_{rj}\right)^{-0.75} \text{ percent}. \quad (15)$$

Figure 2 is an extended version of Deere and Miller approach [1] and will cover very low strength-to-very high strength rocks. A modulus ratio of 500 would mean a minimum failure strain of 0.2%, whereas a ratio of 50 corresponds to a minimum failure strain of 2% as per Eq. (13). Very soft rocks and dense/compacted soils would show often failure strains of the order of 2%. Therefore, the

Table 10 Strength classification of intact and jointed rocks

Class	Description	$\sigma_{ci,j}$, MPa
A	Very high strength	> 250
B	High strength	100–250
C	Moderate strength	50–100
D	Medium strength	25–50
E	Low strength	5–25
F	Very low strength	< 5

Table 11 Modulus ratio classification of intact and jointed rocks

Class	Description	Modulus ratio of rock, $M_{ri,j}$
A	Very high modulus ratio	> 500
B	High modulus ratio	200–500
C	Medium modulus ratio	100–200
D	Low modulus ratio	50–100
E	Very low modulus ratio	< 5

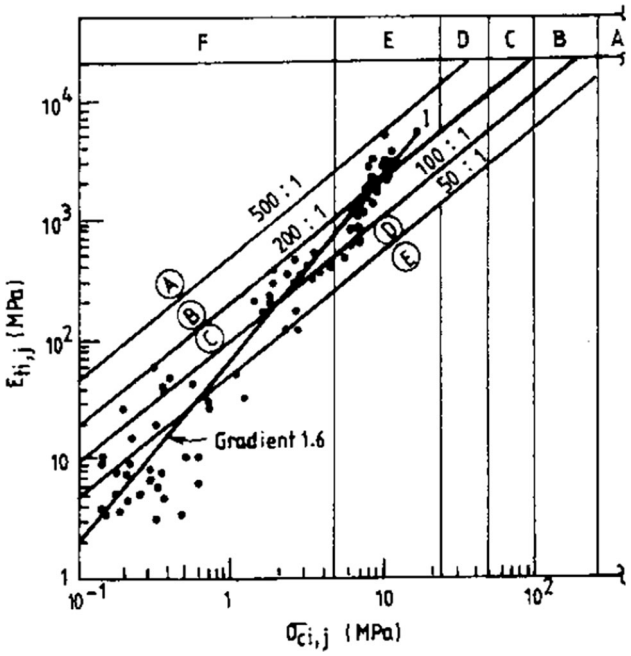

Fig. 2 Influence of jointing on modulus ratio [30]

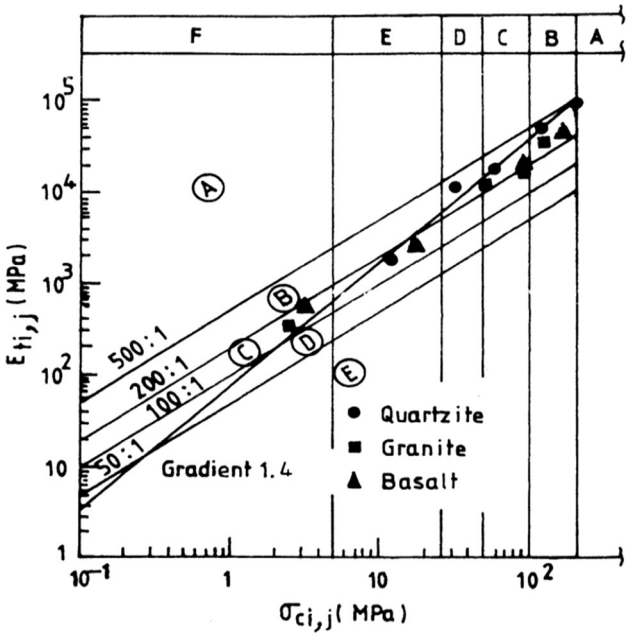

Fig. 3 Influence of weathering on modulus ratio of rocks [31]

modulus ratio of 50 was chosen as the lower limiting value for rocks [29].

In Fig. 2, the location of the intact specimen is shown at "*I*" on the $\sigma_{ci,j}$ and $E_{i,j}$ plot. When the experimental data of σ_{cj} and E_j of the jointed specimens of the same material as that of the intact specimen are plotted, all the points fall along an inclined line originating, say at "*I*", cutting across the constant boundaries of modulus ratio. This suggests that as fracturing continues, the locations represented by σ_{cj} and E_j follow a definite trend [30]. These data are from test specimens, each of which had on an average more than 260 elemental cubes and wedge shape elements. These specimens have undergone either sliding, shearing, splitting or rotational mode of failure.

Unconfined compression tests were also carried out on three weathered rocks, namely quartzite, granite and basalt [31]. These three rocks have gone through different stages of weathering, namely unweathered (i.e., fresh), slightly, moderately, highly and completely weathered. These tests were carried out on five levels of weathering of quartzite and four levels of weathering of both granite and basalt. The values of compressive strength and modulus are presented together for these rocks in Fig. 3. It is interesting to observe that the average line cuts the $M_{rj} = 50$ line at about $\sigma_{cj} = 1$ MPa. Therefore, soil–rock boundary is not only when $\sigma_{cj} = 1$ MPa but also when $M_{rj} = 50$ and $J_f = 300$ per meter [27]; that is, for rock mass $\sigma_{cj} > 1$ MPa, $M_{rj} > 50$, $J_f < 300$.

Ideally when field tests are conducted, the test block is to be isolated from the parent mass by careful cutting and dressing operations to assess σ_{cj} and E_j in the unconstrained condition. Such a test block should have a slender ratio more than one, preferably two. Unfortunately, the data from such tests are rarely available. Whenever some data are available, it is projected to indicate the effect of the specimen size rather than the change in the quality of the rock within the test specimen/block. As the size increases, the number of joints, their inclination, even if the strength along some of the joints remains same, would effect the response of the block. If one compares a value reflected by the large sized test blocks to that of the intact specimen, the values particularly σ_{cj}/σ_{ci} and E_j/E_i would correspond to higher values of J_f. A more recent example is from Natau et al. [32] whose test results from three sizes of specimens ranging from 80 mm to 620 mm were obtained totally in the unconfined state. The average results of σ_{cj} and E_j are presented in Table 12. From these results, σ_{cj} of 620 × 620 × 1200 mm specimen is 0.235 times the value of 80-mm dia. specimen. By extrapolation, the value of compressive strength of NX size, assuming it to represent an intact rock, this ratio works out to be 0.20. The values of

Table 12 Size effect on modulus ratio [32]

Dia. or side, cm	$\sigma_{ci,j}$, MPa	$E_{i,j}$, MPa	$M_{ri,j}$
NX size	50.0[a]	50,000[a]	1000
8.0	42.6	40,000	939
23.5	22.23	7500	337
62.0	10.0	2500	250

[a]Extrapolated from data of larger sizes

σ_{ci} of the NX size works out to be 50 MPa and E_i= 50 GPa. Similarly, the ratio of E_j of 620-mm specimen to the NX size is 1/20. This ratio suggests an average J_f of 230/meter from strength and modulus considerations as per Eqs. (9, 10). The ratio M_{ri} of NX size is 1000, and the M_{rj} of 620-mm-size specimen works out to be 250, suggesting a considerable change in the quality of the rock in the larger size. These data also do confirm that the M_{rj} values should decrease considerably with the decrease in the quality of the rock and not increase, remain constant or vary marginally. Earlier investigations of Rocha [33] also suggested very low values of E_j/E_i as 1/29 for granite, 1/28 for schist, 1/64 for limestone and 1/108 for quartzite.

Confining Pressure Influence

Most of the data of modulus are obtained by conducting tests on limited area in tunnels, in drifts or in boreholes. Even if plate loading tests are conducted on a level surface underground or in open excavation, there is always some degree of lateral confinement. The measured modulus values tend to be higher particularly for weaker rock masses. Such results need to be corrected for lateral confinement to obtain values corresponding to the unconfined condition. When such data are provided, the designer has the freedom to choose or modify the strength and modulus depending upon the in situ stress expected in the field. Using Eq. (16) [34], the influence of confining pressure on E_j can be estimated,

$$E_{j0}/E_{j3} = 1 - \exp\left[-0.10\sigma_{cj}/\sigma'_3\right], \tag{16}$$

where the subscripts 0 and 3 refer to $\sigma'_3 = 0$ and $\sigma'_3 > 0$; σ'_3 is the effective confining stress. For σ_{cj} = 5 MPa, E_{j3} for σ'_3 = 2 MPa confining pressure will be 4 times and for σ'_3 = 1 MPa, it will be 2.3 times of E_{j0}. This is likely to happen in field plate load tests conducted underground on a limited surface area or when lateral in situ stress not being fully released.

The strength criterion for the jointed rocks when σ'_3 is large compared to its tensile strength, σ_t, is given by

$$\left(\sigma'_1 - \sigma'_3\right)/\sigma'_3 = B_j\left(\sigma_{cj}/\sigma'_3\right)^{\alpha j}, \tag{17}$$

where σ'_1 and σ'_3 are major and minor principal stresses, respectively, σ_{cj} is the uniaxial compressive strength of jointed rock obtained from Eq. (9), and α_j and B_j are strength parameters of the jointed rock. The values of α_j and B_j are obtained from Eqs. (18, 19),

$$\alpha_j/\alpha_i = \left(\sigma_{cj}/\sigma_{ci}\right)^{0.5} \text{ and} \tag{18}$$

$$B_i/B_j = 0.13\exp\left[2.04\alpha_j/\alpha_i\right], \tag{19}$$

where α_i and B_i are values of strength parameters obtained from triaxial tests on intact rock specimens for the failure criterion [27, 34]. When Eq. (17) is to be applied for the strength of rock mass along the periphery of excavation, i.e., when $\sigma'_3 \triangleq 0$, the tensile strength, σ_t, of rock mass has to be considered in the denominator along with σ_3 as per the original expression for the strength of rock [27]. One way to assess σ_t for rock mass would be to consider proportional reduction from the intact rock σ_t, similar to the proportional reduction in compressive strength of intact rock.

Prediction of Rock Mass Responses with Joint Factor

Elasto-plastic Analysis

The power house complex of Nathpa Jhakri hydropower project in North India consists of two major openings, i.e., machine hall $216 \times 20 \times 49$ m^3 (length × width × height) with an overburden of 262.5 m and a transformer hall $198 \times 18 \times 29$ m^3 which is located downstream of the machine hall. The in situ stress for the rock was determined using hydraulic fracturing technique. The vertical stress was found to be 5.89 MPa with an in situ stress ratio of 0.8035. The constitutive model based on disturbed state concept [35] was used to characterize complete stress–strain behavior of the intact and rock mass. Material parameters for the model were determined for the rock specimens as indicated in Table 13 [36]. The rock mass was discretized into 364 eight nodded elements and 1167 nodes, keeping in view the various stages of excavation.

Strength and modulus of the jointed rock mass, quartz mica, were determined with joint factor J_f [37] to carry out the finite element analysis of the powerhouse cavern by considering strain softening behavior of rock mass. The failure criterion based on J_f [27] was adopted to estimate the strength under different in situ stresses. The analysis was carried out using computer code DSC-SST-2D developed by Desai [38]. Twelve stages of excavation were used in the study.

The predicted values of the displacements by FEM were compared with the observed values at six locations and found to be within the range of measured deformations at five out of six locations (Table 14).

Equivalent Continuum Modeling (ECM)

Using the strength, modulus and failure strain relations for rock mass with J_f and the corresponding values of intact rock, a few cases were analyzed [39–42]. The tangent elastic modulus of intact rock was represented by confining

Table 13 Intact and rock mass properties of Quartz Mica Schist [36]

σ_{ci}, MPa	E_i, MPa	J_f	σ_{cj}, MPa	E_j, MPa	α_i	B_i	α_j	B_j
15.71	8591	21.9	13.18	6677	0.38	2.1	0.35	1.76

Table 14 Comparison of predicted and observed deformations at the powerhouse cavern boundary, [36]

Stages	Excavation		Instrumented El. (m)	Deformation (mm)	
	From El. (m) to El. (m)			Predicted	Observed[a]
1	Widening of central adit		1024	10.4	13–18
2	Widening of central adit		1022	12.0	6–12
3	1018	1006	1022	0.6	− 1.3 to + 2.5
4	1006	1000	1018	3.5	1–4
5	1000	975	1006	23.7	10–45
6	983	975	996	9.4	1–3

[a]Observed deformation ranges indicate movements along the length of the cavern boundary

stress-dependent hyperbolic relation [43]. A numerical model was developed from an existing finite element code for a nonlinear soil–structure interaction program to account for material nonlinearity of both the intact and jointed rocks.

This model was incorporated in the commercial finite difference code FLAC. A FISH function was written to incorporate joint factor model with Duncan–Chang non-linear hyperbolic relationships in FLAC. The model has been applied to two large power station caverns, one in Japan and the other in the Himalayas, and to a slope at Kiirunavaara mine in Sweden. For validation purposes, the finite element analysis was applied to predict the response of jointed rocks of sandstones, granite and gypsum plaster and compared with the experimental results. Only sample stress–strain plots for multiple jointed specimens of Agra sandstones are shown in Fig. 4 and for block jointed specimens of gypsum plaster [44] for different confining pressures are shown in Fig. 5 along with the experimental results [40].

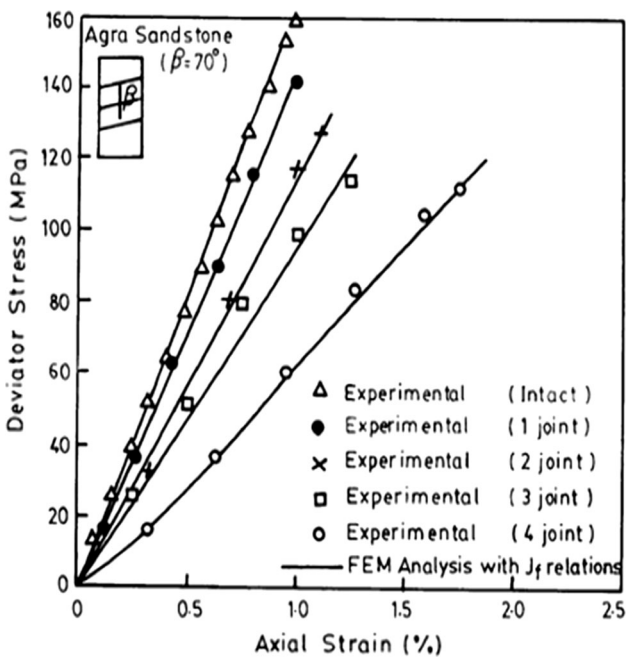

Fig. 4 Stress–strain plots for intact and multiple jointed specimens, for confining pressure 5.0 MPa, experimental data after Arora [51]

Analysis of Shiobara Power House Cavern

The equivalent continuum model was applied for the analysis of a large cavern in jointed rock mass for the Shiobara power station in Japan [45]. The cavern (Fig. 6) measures 161 m length, 28 m width and 51 m height, located at a depth of 200 m below the ground. The three in situ principal stresses were recorded as 5.0, 3.9 and 2.8 MPa. The reported average intact rock compressive strength and elastic modulus were 83.3 MPa and 42.1 GPa, respectively. The rock mass was characterized as rhyolite consisting of platy and columnar joints. The cross section of the cavern along with the location of the MPBXs is shown in Fig. 6. The jointed rock mass surrounding the cavern has been analyzed by the finite element method using the proposed equivalent continuum approach. Equivalent material properties for jointed rock were modeled using the relations with J_f which was taken as 41, 12 and 111 per meter for joint sets I, II and III, respectively. The variation of relative displacement at the end of different excavation steps with progress of cavern excavation with time–displacement measurements along the measurement line agreed well with the observed values. These

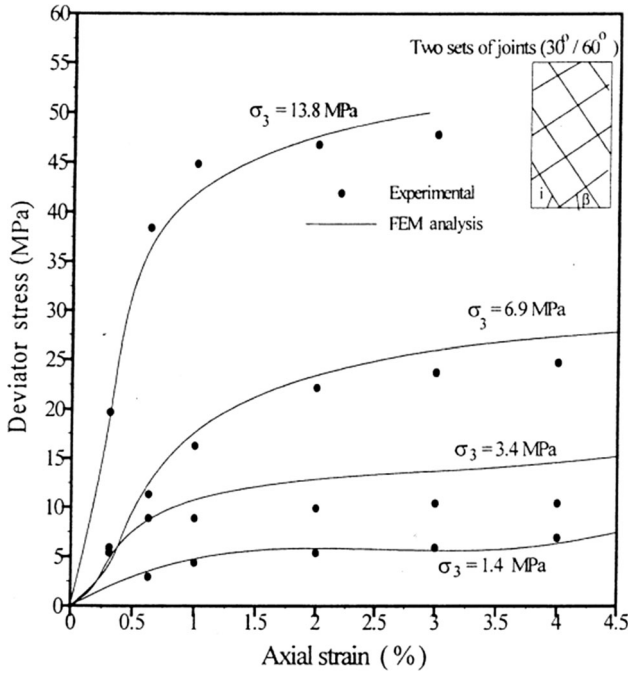

Fig. 5 Calculated and experimental stress–strain plots for block jointed specimen of gypsum plaster for different confining pressures [41]

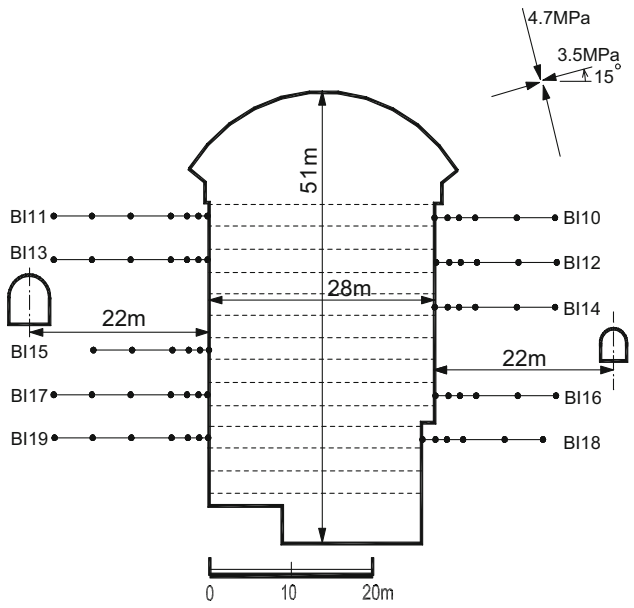

Fig. 6 Cross section of cavern and location of displacement transducer [45]

are presented here only for B110 and B111 in Figs. 7 and 8. The variation of relative displacements from FEM and as measured, [45], at the completion of whole excavation along a measurement line were compared for B117 (Fig. 9) [41]. The parameter r was chosen from Table 8, based on intact rock density.

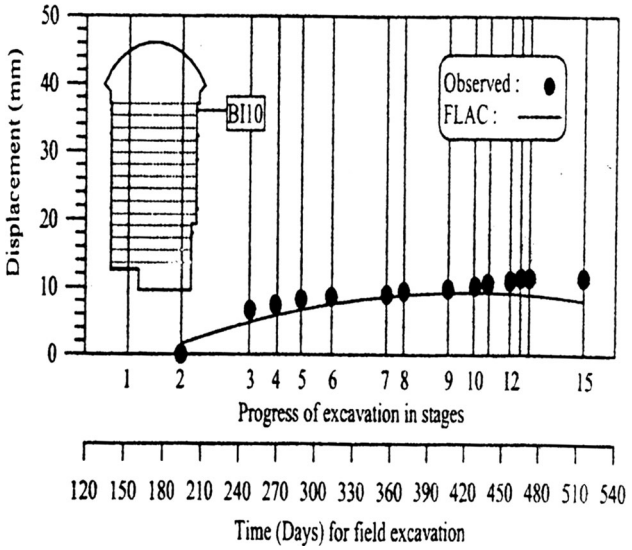

Fig. 7 Time history of displacements near the cavern wall along measurement line B110 [41]

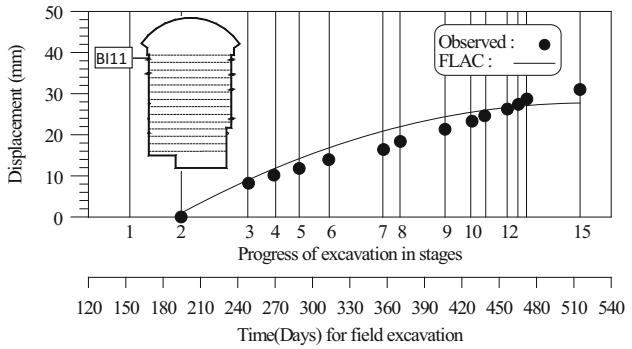

Fig. 8 Time history of displacements near the cavern wall along measurement line B111 [41]

Analysis of Kiirunavaara Mine, Sweden

The Kiirunavaara mine, which is 4000 m long, with an average width of 90 m, is located 144 km north of the arctic circle in the city of Kiruna in North Sweden. The magnetic iron ore body is relatively strong surrounded by competent quartz porphyry on the hanging wall and syenite porphyry on the footwall. The rock mass has three joint sets. One joint set is oriented roughly parallel to the ore body as the other two strikes obliquely to the ore body. All joints dip fairly steep, 60°–90°. The locations where the first set of cracks were observed in 1985 were mapped by Sjoberg [46].

The value of joint factor (J_f) was obtained as 13. The parameter r was chosen from Table 8. The total size of the model used was 2000 × 1300 m [41]. Sequential mining was simulated in the FLAC by modeling the excavated

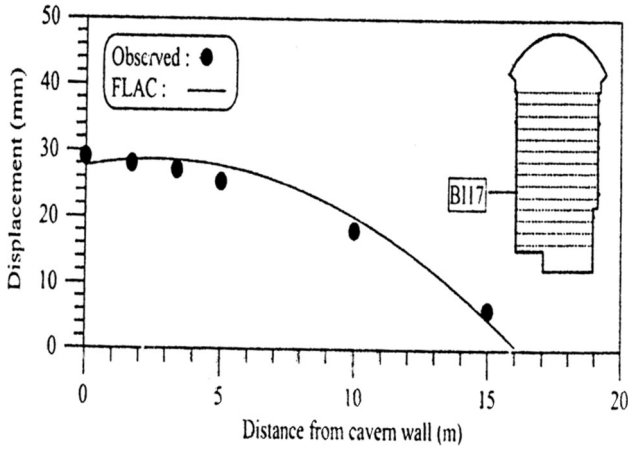

Fig. 9 Displacement along measurement line B117 at the completion whole excavation [41]

material with null model and solving after each stage of excavation. Failure was only observed from the concentration of shear strains in the model on the foot wall. The paths of concentrated shear strains represented the failure surface in the model. The failure thus simulated by the numerical model using practical equivalent continuum approach was compared with the failure observations in the field. Shear failure was observed in the footwall of the model while excavating at the mining level of − 586 m, agreeing with the field observations as reported by Sjoberg [46]. Typical failure surface for the mining step of − 586 m is presented in Fig. 10. The intact rock parameters are indicated in Table 15.

Analysis of Nathpa Jhakri Power House Cavern

This cavern was also analyzed by Sitharam and Madhavi Latha [40]. The finite difference grid used for the analysis was of size 210 m × 450 m with 1320 rectangular zones. The excavation steps were simulated in the numerical analysis (FLAC 2D), and the locations of the installation of extensometers were identified for obtaining the displacements for comparison with the measured displacements from instrumentation of the cavern. The variation of displacements with time is also obtained from numerical analysis by solving for equilibrium after each excavation step. Comparison of the observed and predicted deformations along the measurement line at different locations for various excavation levels after the completion of excavation is presented in Table 16. The joint factor was estimated as 22 per meter for the analysis, and the value of r was chosen from Table 8. And other parameters of intact rock were as indicated in Table 13. The ranges of deformations indicate movements of measuring points on the face of the cavern along its length at these elevations. The variation of displacements with time was also obtained from numerical analysis by solving for equilibrium after each stage of excavation step. Figure 11 shows comparison of measured and predicted displacements at two locations behind the face of the power house cavern, with time using joint factor linked relationships [27].

Abutment Stability of Chenab Bridge

Slope stability analysis of the right abutment (359 m high) at Kauri side of Chenab river between Katra and Laole, Jammu and Kashmir, India, was carried our using FLAC of plane strain case for pseudo-static approach with earthquake intensity of 6.5 [47], Sitharam and Maji [48]. With J_f values and intact rock properties, σ_{cj}, E_j, hyperbolic stress–strain response, c_j and ϕ_j for the rock mass are computed. By applying varying factors of safety to c_j and tan ϕ_j, failure conditions in the slope were determined. The rock parameters adopted were: $\sigma_{ci} = 115$ MPa, $E_i = 65$ GPa, $J_f = 320$, $\sigma_{cj} = 5.38$ MPa, $E_j = 4.34$ GPa, $c_j = 1.785$ MPa, $\phi_j = 23^\circ$. The static factor of safety achieved was 1.86.

Stress–Strain Response

Arunakumari and Latha [49] introduced user-defined FISH functions to incorporate relations based on J_f into the explicit finite difference code FLAC (version 4.0, ITASCA 1995) to simulate exact joint behavior. Adopting hyperbolic formulation of stress–strain response of jointed rock, estimated elastic initial tangent modulus as per Duncan and Chang [43], they predicted stress–strain, strength envelopes and variation of strength with joint orientation of tested specimens. A very good agreement has been shown.

Joint Factor in ANN Model

By constructing an ANN model, stress–strain response and variation of E_j/E_i with J_f were predicted for jointed rocks, by specifying intact rock properties, σ_3, J_f and axial strain as inputs [50]. Out of number of cases presented by them, only stress–strain curves predicted by equivalent continuum (with J_f) and ANN models are presented in Fig. 12 with experimental results of block jointed gypsum plaster [44]. Figure 13 shows the predictions as per ANN with experimental results of Agra sandstone [51].

Comparison of ECM and DCM

More recently, Latha and Garaga [52] have predicted the stress–strain response of jointed specimens of six different rock types with varying joint inclination and joint frequency in triaxial compression adopting equivalent continuum method (ECM) based on joint factor and all the related equations [26, 34] and discrete continuum method

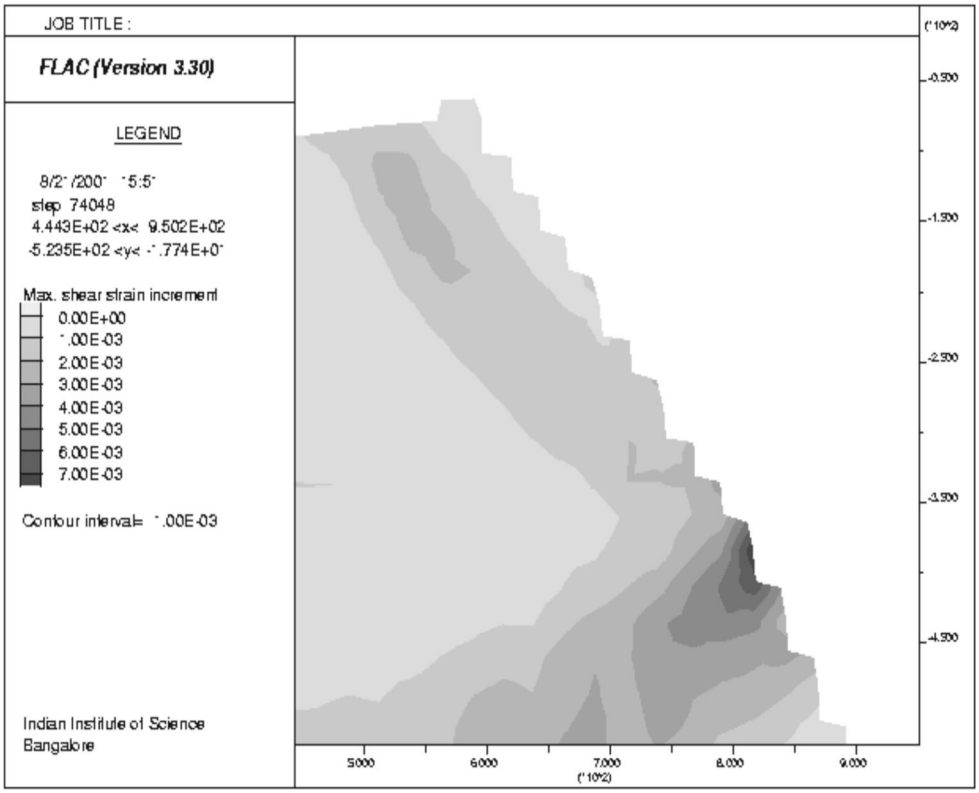

Fig. 10 Shear strains for FLAC model for − 586 m mining level [41]

Table 15 Parameters for numerical model of Kiirunavaara mine [40, 46]

Parameters	Hanging wall	Foot wall	Ore body
σ_{ci}, MPa	100	140	115
E_i, GPa	19	18	17
Density, kg/m^3	2700	2800	4700

Table 16 Measured and predicted deformations at Nathpa Jhakri cavern [41]

Stage	Location of MPBX, ELm	Deformation along the line (mm)	
		Observed	Predicted *FLAC-2D*
1	1024	13–18	10–14.0
2	1022	6–12	8.2–13.5
3	1022	− 1.3 to 2.5	1–2.3
4	1018	1–4	1.4–3.7
5	1006	10–45	13–42.2

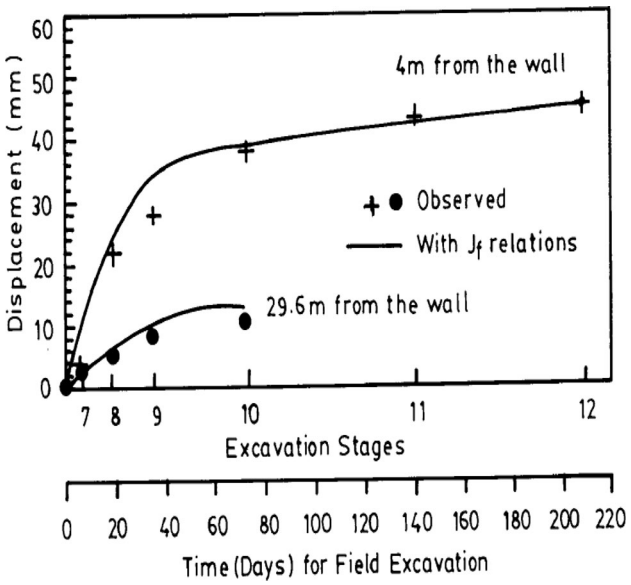

Fig. 11 Comparison of displacements along measurement line for powerhouse cavern [42]

(DCM). Both the approaches predict reasonably close responses of jointed specimens and demonstrated that ECM can be adopted without compromising much on the accuracy. They applied ECM to Shimizu tunnel No. 3, which is a part of the new Tomei Express way in Japan. The tunnel length is 1.2 km located at a depth of 83 m below ground level in soft sandstone. Three joint sets exist, namely bedding plane, dipping 28°, random cross joints dipping 58° and near vertical joint dipping 88°. The horizontal stress is 2.03 MPa, and the vertical stress is 1.73 MPa. It was decided to excavate the tunnel in three stages, i.e.,

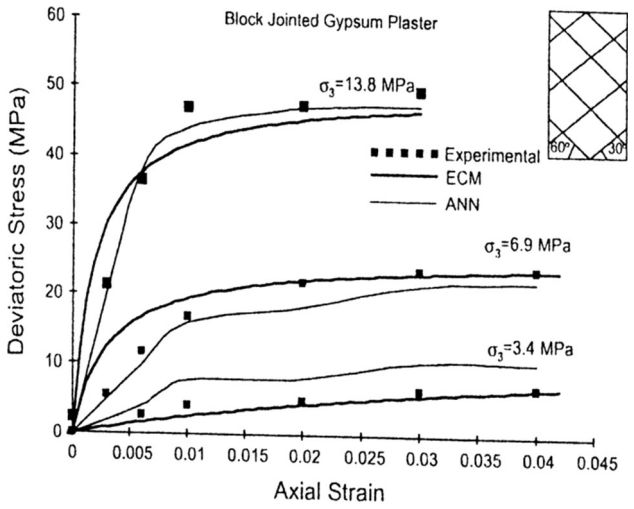

Fig. 12 Comparison of stress–strain curves predicted by ECM and ANN with experimental values for block jointed gypsum plaster [50]

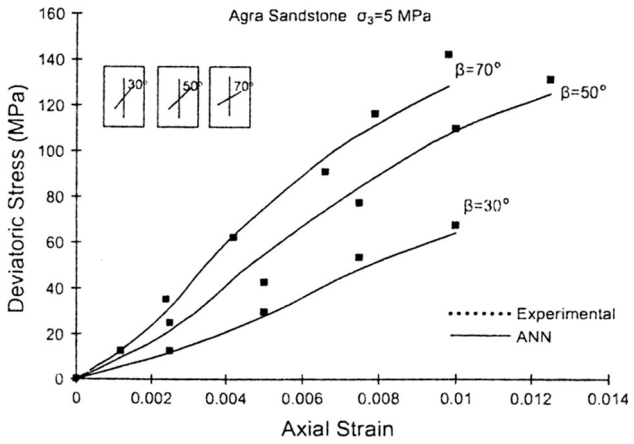

Fig. 13 Effect of joint orientation on the stress strain response of Agra sandstone [50]

Table 17 Comparison of displacements from numerical methods with field measurements [53]

Location	Displacements observed in field, mm	Displacements predicted by UDEC, Vardakos [53], mm	Displacements predicted by FLAC, Latha and Garaga [52], mm
C	9.5	15.0	15
D	13.0	12.4	13.2
H	12.0	8.9	13.2
E4	1.0	3.7	5.0
E2	3.0	8.8	5.0
G1	15.0	13–18	15.0
E1	8.0	12.2	13.2
E3	3.0	5.6	5.0

pilot tunnel, top heading and bottom benching; the tunnel being 12 m high and 18 m wide. The soft sandstone has $\sigma_{ci} = 60\,\text{MPa}$, $E_i = 3000\,\text{MPa}$, $c_i = 2\,\text{MPa}$ and $\Phi_i = 38^\circ$. The joint factor, J_f, worked out for the critical joint dipping at 28° is 111, as per Ramamurthy [26, 34]. The detailed analysis carried out by ECM using FLAC to predict displacements at various locations along the crown shows good agreement with the observed values and those predicted by Vardakos [53] using UDEC, as indicated in Table 17.

Penetration Rate of TBMs P_R

Whether it is in Q_{TBM} [54], RMR or any other rock mass classification linked to P_R, the modulus of rock has been ignored (Fig. 14). For producing indentation by crushing under the tip of the cutter, compressive and tensile strengths are important. In doing so, whatever deformation/penetration is produced will depend on the modulus response of rock mass. It is therefore very essential that the modulus of rock mass be considered. More precisely, the modulus ratio to account for the combined influence of compressive strength (σ_{cj}) and modulus (E_j) of the rock mass, i.e., $M_{rj} = E_j/\sigma_{cj}$. Basically under each cycle of boring by TBM, the various other major factors which control P_R are included in the following Eq. (20). This equation is dimensionally correct and predicts P_R value per meter of advance of boring as indicated below [55],

$$P_R = \frac{(T/A)\cdot(\sigma_{ci}/\sigma_t)\cdot R\cdot N\cdot(\text{DRI}/100)\cdot s}{p_o\cdot M_{rj}} \tag{20}$$

where T net thrust, T; A area of the cutter head, m^2; σ_{ci} compressive strength of intact rock, MPa; σ_t tensile strength of intact rock, MPa; R number of rotations of cutterhead, per hour; N number of cutters, per m^2; DRI drilling rate index based on compressive strength of intact rock (Fig. 15) NTH [56]; S unit length of drilling, m; p_o mean biaxial stress on the cutting face, T/m^2 (or taken as density of rock mass times over burden height); M_{rj} modulus ratio of rock mass, $(= E_j/\sigma_{cj})$,

In Eq. (20), the influence of seepage pressure is not considered, since most of the seepage pressure is dissipated at the cutting face due to the presence of fractures, joints, etc. The seepage pressure acting through the intact rock will be negligible anyway on the cutting face. The rock parameters are to be obtained under saturated condition, if seepage exists. If seepage pressure exists, effective trust should be considered

The ratio (σ_{ci}/σ_t) takes care of inherent anisotropy in the intact rock and also its brittleness. When the gouge material thickness is less than 5 mm, the blocks formed in the rock mass may remain tight/interlocked and may not

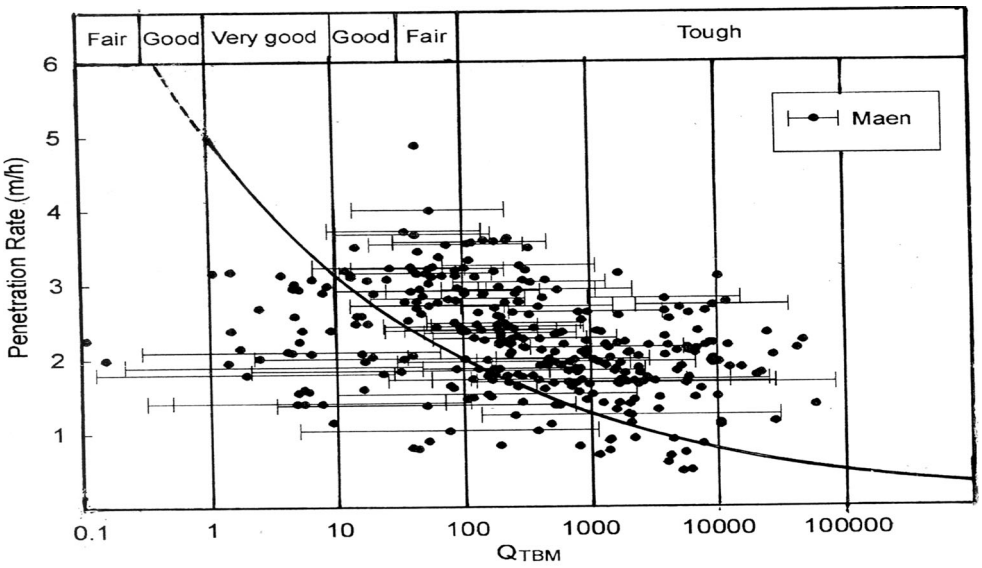

Fig. 14 Scatter of P_R with Q_{TBM} for Maen tunnel

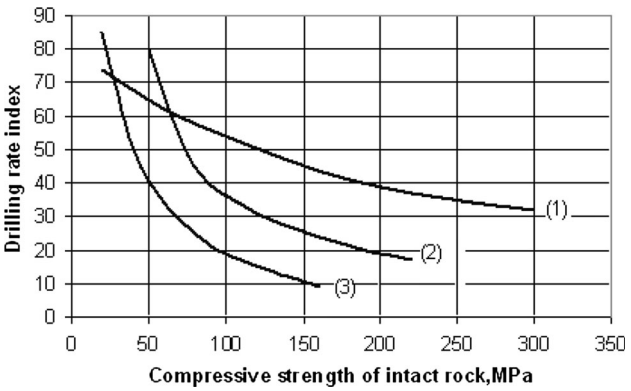

Fig. 15 Compressive strength versus DRI: (1) Granite, Quartzite, Sandstone, Siltstone (coarse to fine grained); (2) Mica schist/Mica gneiss; (3) Phyllite/Shale (extended curve)

get dislodged during boring operation. But when the gouge material thickness is more than 5 mm, rock blocks get dislodged and may damage the cutters. To take into consideration the thickness of gouge in the estimation of J_f, equivalent number of joints are estimated by dividing the thickness of gouge (in mm) by 5 mm, which is the minimum thickness of gouge to be effective [27].

Case Study for Penetration Rate

Excellent data were collected by Sapigni et al. [57] from NW Alps. These data are applied to verify Eq. (20). What all the data are required for this presentation is reported by Sapigni et al. for metabasite in Maen tunnel and for micaschist and metadiorite in Pieve tunnel for various values of RMR. The scatter of P_R values with Q for these rock types are shown in Fig. 15. The RMR values given have been converted to J_f, joint factor. The values of compressive strength, tensile strength and modulus values for the three rocks are given in Table 18. The basic tunnel equipment data of Maen tunnel and that of Pieve tunnel are given in Table 19 for use in Eq. (20). Table 20 gives minimum, average, maximum values of M_{ri} as per Table 18 and also values of M_{rj}/M_{ri} for different values of RMR and J_f. Tables 21, 22 and 23 present actual range of P_R versus J_f, RMR and the values of P_R estimated from

Table 18 Properties of intact rocks, Sapigni et al. [57]

Description	Uniaxial compressive strength, MPa	Tensile strength, MPa	Modulus value, GPa
Maen tunnel, Metabasite	180 (104–289)	15 (9–29)	65 (35–94)
Pieve tunnel, Micaschist Metadiorite	124–215 171–221	5–9 8–13	28 46–100

Table 19 Tunnel Equipment Data (Sapigni et al. [57])

Description	Mean tunnel	Pieve tunnel
Excavated diameter, m	4.20	4.05
Numbers of cutters	36	27
Cutter spacing, mm	66	75
Cutter diameter, mm	432	432
Max thrust, T	792	460.2
Boring stroke, m	1.5	0.63
Cutterhead rotation, rph	660, 330	678
Cutterhead curvature	Domed	Flat
TBM type	Open	Double shield

Table 20 Values of M_{rj}/M_{ri} for J_f (or RMR)

				Min.	Avrg.	Max.
Metabasite	94	30	0.900	356	361	325
Maen tunnel	84	80	0.756			
	74	130	0.634			
	66	170	0.550			
	55	225	0.455			
Mica schist Pieve tunnel	83	85	0.743	130	164.7	225.8
	75	125	0.646			
	68	160	0.570			
	57	215	0.471			
	50	250	0.417			
	35	325	0.320			
Meta diorite	92	40	0.869	269	372.5	221
Pieve tunnel	84	80	0.756			
	74	130	0.634			
	66	170	0.550			
	53	235	0.439			

Eq. (20) for minimum, average and maximum values of M_{rj}. A comparison of the calculated and field measured mean P_R values in these three tables for 16 rock types clearly suggests a good agreement. By considering lower M_{ri} values, the P_R values nearly match with the maximum values of P_R from field. Adoption of maximum values of M_{rj} will suggest lower values in the range. With the adoption of average values of M_{ri} in Eq. (20), the P_R values estimated would suggest mean P_R values from the field. In Table 19 for Maen tunnel, the rotation of cutterhead has been at two rates, namely 660 rph and 330 rph. By considering rph of 330 particularly for J_f of 170 and 225, the P_R values will be halved and will be within the actual range in the field.

Table 21 Mean tunnel, metabasite, rock mass density—2.6 T/m^3, average overburden—400 m, cutterhead rotation—660 rph

RMR	Joint factor J_f per m	P_R, m/h from Eq. (20)			Actual range P_R, m/h
		Min. M_{rj}	Avrg. M_{rj}	Max. M_{rj}	
94	30	1.9	1.5	0.9	0.3–1.4
84	80	2.2	1.7	1.0	1.3–2.0
74	130	2.6	2.1	1.2	1.0–1.8
66	170	3.1	2.4	1.4	1.3–2.1
55	225	3.7	2.9	1.5	1.5–2.0

Table 22 Pieve tunnel, micaschist, rock mass density—2.6 T/m^3, average overburden—500 m, cutterhead rotation—678 rph

RMR	Joint factor J_f per m	P_R, m/h from Eq. 20			Actual range P_R, m/h
		Min. M_{rj}	Avrg. M_{rj}	Max. M_{rj}	
83	85	1.7	1.7	1.5	1.2–2.2
75	125	2.0	1.9	1.8	1.6–2.5
68	160	2.4	2.2	2.0	2.0–2.8
57	215	2.7	2.7	2.4	2.1–3.3
50	250	3.0	3.1	2.8	2.3–3.4
35	325	3.9	4.0	3.5	2.5–3.5

Table 23 Pieve tunnel, metadiorite, rock mass density—2.6 T/m^3, average overburden—500 m, cutterhead rotation—678 rph

RMR	Joint factor J_f per m	P_R, m/h from Eq. 20			Actual range P_R, m/h
		Min. M_{rj}	Avrg. M_{rj}	Max. M_{rj}	
92	40	1.6	0.9	0.37	0.8–1.25
84	80	1.9	1.1	0.44	0.8–1.70
74	130	2.2	1.3	0.51	1.4–2.2
66	170	2.4	1.4	0.59	1.5–2.4
53	235	3.0	1.7	0.70	1.9–2.15

It has been reported by many investigators that particularly for $J_f > 200$ decrease in P_R is generally observed. This is mainly due to the dislodging of rock blocks hindering P_R values. Such decrease in P_R is indicated from the data of Sapigni et al. [57]. In such situations, the operators usually reduce the rotations of TBM.

The special advantage of adopting Eq. (20) for predicting P_R is that all the input data are factual and from test conducted on the rocks as per approved practice. It is dimensionally correct compared to other prevailing expressions. The P_R may be calculated per meter of boring in a specified length having similar formation. Assessment of P_R per meter length of tunnel is specified because the J_f value is estimated per meter length. On the basis of this, one could estimate average P_R in each zone and then an overall estimation of the P_R or for the entire length of the tunnel would result. Since an excellent site investigation of a tunnel alignment is essential for its successful execution with TBM, Eq. (20) will certainly be very handy in predicting P_R.

Discussion

Equation (20) is simple and dimensionally in order unlike all other expressions in vogue to predict P_R. It takes into consideration the basic parameters of TBM, intact rock, rock mass, in situ stress and drilling rate index which is linked to compressive strength of intact rock. The prediction of P_R has been made for 16 rock types from Mean and Pieve tunnels, and a very good agreement is observed with the field data. The thrust of TBMs as given for these tunnels has been adopted in the estimation of P_R; it is the maximum thrust. The net values of thrust may be some what less by 10–15%; the P_R values will not be drastically altered. At the most, a correction factor of 1.2–1.5 may have to be applied in Eq. (20) to obtain more realistic values of P_R by considering net thrust. Rest of the data adopted are either measured or taken from well-established relationships. A reduction of 10%, 25% and 40% in the calculated P_R may have to be made for values of J_f values of 250, 300 and 350, respectively, to account for the decrease in P_R for $J_f > 200$ due to dislodging of rock blocks and slow down of TBM rotations.

Conclusions

A critical examination of the most commonly adopted rock mass classifications, namely RMR, Q and GSI, has revealed that the compressive strength and modulus values suggested need some definite modifications based on the modulus ratio criterion, which defines the quality of rock mass. In practice, the modulus ratios of rock masses have been found to be much higher than those of intact rocks. Predicted deformations did not agree with the field measured values. Application of joint factor, J_f, to solve some field problems and prediction of the response of laboratory tests seems to be encouraging. The relationships based on J_f for rock masses appear to be more realistic since these are based on experimental verifications. A unified rock mass classification based on modulus ratio concept, applicable to both intact and mass of rocks, would give better assessment of engineering responses. Consideration of modulus ratio in predicting the penetration rate of TBMs seems to be more realistic, simple and easy to apply.

Acknowledgements Authors thank the IGS Executive Committee for offering the opportunity to present this Sixth Terzaghi Oration, M/S Ferro co for initiating and supporting this Oration activity, the local chapter of IGS at Indore for making arrangements, Prof. Seetharam and Prof. Madhavi Latha promoting our researching findings in predicting the performance of rocks, my research scholars who guided research in characterizing the rock mass, and also my colleagues for establishing a healthy environment at IIT Delhi for nurturing Rock Mechanics activity.

References

1. Deere DU, Miller RP (1966) Engineering classification and index properties for intact rocks. Technical report no. AFNL-TR-65-116, Air Force Weapons Laboratory, New Mexico
2. Hobbs NB ((1975) Factors effecting the prediction of settlement of structures on rock: with particular reference to chalk and Triass in settlement of structures. In: Proceedings of the conference on settlement of structures, Prentech Press, pp 579–610

3. Bieniawski ZT (1973) Engineering classification of jointed rock masses. Trans S Afr Inst Civ Eng 15(12):335–344
4. Barton N, Lien R, Lunde J (1974) Engineering classification of rock masses for the design of tunnel support. J Rock Mech 6(4):189–236
5. Hoek E (1994) Strength of rock and rock masses. ISRM News J 2(2):4–16
6. Hoek E, Brown ET (1997) Practical estimates of rock mass strength. Int J Rock Mech Min Sci 34(8):1165–1186
7. Bieniawski ZT (1976) Rock mass classification in rock engineering. In: Bieniawski ZT (ed) Proceedings of the symposium on exploration for rock engineering, vol 1. A.A. Balkema, Rotterdam, pp 97–106
8. Serafim JL, Pereira JP (1983) Consideration of the geomechanics classification of Bieniawski. In: Proceedings of the international symposium on engineering geology and underground construction, Lisbon, Portugal, no II, pp 33–44
9. Barton N (2002) Some new *Q*-value correlations to assist in site characterisation and tunnel design. Int J Rock Mech Min Sci Geomech Abstr 39(2):185–216
10. Moretto O, Pistone RES, DelRio JC (1993) A case history in Argentina—Rockmech. For underground works in pump storage development of Rio Grande No. 1. In: Hudson JA (ed) Comprehensive rock engineering, vol 5. Pergamon Press Ltd., Oxford, pp 159–192
11. Barla G (1993) Case study of rock mechanics in Masua mine, Italy. In: Hudson JA (ed) Comprehensive rock engineering, vol 5. Pergamon Press Ltd., Oxford, pp 291–334
12. Hoek E, Moy D (1993) Design of large power house caverns in weak rocks. In: Hudson JA (ed) Comprehensive rock engineering, vol 5. Pergamon Press Ltd., Oxford, pp 85–110
13. Yu C, Liu SC (1993) Power caverns of Mingtan pumped storage project, Taiwan. In: Hudson JA (ed) Comprehensive rock engineering, vol 5. Pergamon Press Ltd., Oxford, pp 111–131
14. Ermekov TM, Abuov MG, Shashkin VN, Freidin AM, Uskov VA (1985) Providing of stability of horizontal mine working in soft rock. In: Proceedings of the 8th international congress on ISRM, Japan, vol 2, pp 671–674
15. Zhou Y, Zhao J, Cai JG, Zhang XH (2003) Behaviour of large-span rock tunnels and caverns under favourable horizontal stress conditions. In: Proceedings of the 10th international congress on ISRM, Johanesburg, vol 2, pp 1381–1386
16. Stabel B, Samani FB (2003) Mashed-e-soloiman hydroelectric power project, rock engineering investigations, analysis, design and construction. In: Proceedings of the 10th international congress on ISRM, Johanesberg, vol 2, pp 1147–1154
17. Tabanrad R (2003) Monitoring and stability analysis of intake tunnels, Karun III hydroelectric power project. In: Proceedings of the 10th international congress on ISRM, Johanesberg, vol 2, pp 1189–1193
18. Lim H, Kim CH (2003) Comparative study on the stability analysis methods for underground pumped power house caverns in Korea. In: Proceedings of the 10th international congress on ISRM, Johanesberg, vol 2, pp 783–786
19. Carvalho JL, Kennard DT, Lorig L (2002) Numerical analysis of east wall of Toquepala mine, Southern Andes of Peru. In: Proceedings of EUROCK, Lisbon, pp 615–625
20. Clark IH (2006) Simulation of rock mass strength using ubiquitous joints. In: Hart R, Varona P (eds) Proceedings of the 4th international FLAC symposium on numerical modeling in geomechanics, Miniapolis
21. Lorig LJ (2007) Using numbers from geology, keynote lecture. In: Proceedings of the 11th international congress on ISRM, Lisbon, vol 3, pp 1367–1377
22. Read JRL (2008) Large open pit project, keynote lecture. In: Proceedings of the international symposium on 6ARMS, New Delhi, pp 119–131
23. Sari M, Karpuz C, Ayday C (2010) Estimating rock mass properties using Monte Carlo simulation: Ankara andesites. Comput Geosci 36:959–969
24. Richards L, Read SAL (2007) Newzealand Greywacks characteristics and influences on rock mass behaviour. In: Proceedings of the 11th international congress on ISRM, Lisbon, vol 1, pp 359–364
25. Hoek E, Diederichs MS (2006) Empirical estimation of rock mass modulus. Int J Rock Mech Min Sci 43(2):203–215
26. Bronshteyn VI, Zhukov VN, Yufin SA, Zertsalov MG, Ustinov DV (2007) Proceedings of the 11th international congress on ISRM, Lisbon, vol 2, pp 1015–1018
27. Ramamurthy T (2001) Shear strength responses of some geological materials in triaxial compression. Int J Rock Mech Min Sci 38:683–697
28. Walsh JB, Brace WF (1966) Elasticity of rock: a review of some recent theoretical studies. Rock Mech Eng Geol 4(4):283–297
29. Ramamurthy T (2004) A geo-engineering classification for rocks and rock masses. Int J Rock Mech Min Sci 41(1):89–101
30. Singh M, Rao KS, Ramamurthy T (2002) Strength and deformational behaviour of a jointed mass. J Rock Mech Rock Eng 35(1):45–64
31. Gupta AS, Rao KS (2000) Weathering effects on the strength and deformational behaviour of crystalline rocks under uniaxial compression state. Int J Eng Geol 56:257–274
32. Natau O, Fliege O, Mutcher TH, Stech HJ (1995) True triaxial tests of prismatic large scale samples of jointed rock masses in laboratory. In: Proceedings of the 8th international congress on rock mech, Tokyo, vol 1, pp 353–358
33. Rocha M (1964) Mechanical behaviour of rock foundations in concrete dams. In: Transactions, 8th congress on large dams, Edinburgh, paper R-44, Q.28, pp 785–832
34. Ramamurthy T (1993) Strength and modulus responses of anisotropic rocks. In: Hudson JA (ed) Chapter 13, comprehensive rock engineering. Pergamon Press Ltd., Oxford, pp 313–329
35. Desai CS (1994) Hierarchical single surface and disturbed state constitutive models with emphasis on geotechnical application. In: Saxena KR (ed) Chapter 5 in geotechnical engineering. Oxford & IBH Pub. Co., New Delhi
36. Varadarajan A, Sharma KG, Desai CS, Hashemi M (2001) Constitutive modelling of a schistose rock in the Himalaya. Int J Geomech 1(1):83–107
37. Varadarajan A, Sharma KG, Desai CS, Hashemi M (2001) Analysis of a powerhouse cavern in the Himalaya. Int J Geomech 1(1):109–127
38. Desai CS (1997) Manual for DSC-SST-2D: computer code for static and dynamic solid, structure and soil-structure analysis, Tucson, Arizona
39. Sitharam TG, Sridevi J, Shimizu N (2001) Practical equivalent continuum characterization of jointed rock masses. Int J Rock Mech Min Sci 38:437–448
40. Sridevi J, Sitharam TG (2000) Analysis of strength and moduli of jointed rocks. Geotech Geol Eng 18:3–21
41. Sitharam TG, Madhavi Latha G (2002) Simulation of excavation in jointed rock masses using practical equivalent continuum model. Int J Rock Mech Min Sci 39:517–525
42. Latha GM, Sitharam TG (2004) Comparison of failure criteria for jointed rock masses. Int J Rock Mech Min Sci 41:3 **(proceedings of sinorock symposium paper 2B08, CD-ROM)**
43. Duncan JM, Chang CY (1970) Non-linear analysis of stress and strain in soil. J Soil Mech Found Eng ASCE 5:1629–1652
44. Brown ET, Trollope DH (1970) Strength of model of jointed rock. J Soil Mech Found Div ASCE 96(SM2):685–704

45. Horii H, Yoshida H, Uno H, Akutagawa S, Uchida Y, Morikawa S, Yambe T, Tada H, Kyoya T, Fumio I (1999) Comparison of computational models for jointed rock mass through analysis of large scale cavern excavation. In: Proceedings of the 9th international congress on ISRM, Paris, vol 1, pp 389–393
46. Sjoberg S (1999) Analysis of large scale rock slopes. Doctoral thesis, Department of Civil and Mineral Engineering, Lulea University of Technology, Sweden
47. Sitharam TG, Maji VB, Varma AK (2005) Equivalent continuum analyses of jointed rock mass. In: 40th US rock mechanics symposium, 25–29 June, Anchorage, Alaska, paper no. 05-776 (in CD ROM)
48. Sitharam TG, Maji VB (2007) Slope stability analysis of a large slope in rock mass: a case study. In: Proceedings of the 11th international congress on ISRM, Lisbon, vol 2, pp 1185–1188
49. Arunakumari G, Latha GM (2007) Effect of joint parameters on stress–strain response of rocks. In: Proceedings of the 11th international congress on ISRM, Lisbon, vol 1, pp 243–246
50. Garaga S, Latha GM (2010) Intelligent prediction of stress–strain response of intact and jointed rocks. Comput Geotech 37:629–637
51. Arora VK (1987) Strength and deformational behaviour of jointed rocks. Ph.D. Theses, Indian Institute of Technology Delhi
52. Latha MG, Garaga A (2012) Elasto-plastic analysis of jointed rocks using discrete continuum and equivalent continuum approaches. Int J Rock Mech Min Sci 53:56–63
53. Vardakos S (2003) Distinct element modeling of Zhimizu tunnel no. 3 in Japan. MS Thesis, Virginia Polytechnic Institute and State University, Blacburg
54. Barton N (1992) TBM performance in rock using Q_{TBM}. Tunn Tunn Int Milan 31:41–48
55. Ramamurthy T (2008).Penetration rate of TBMs. In: Proceedings of world tunneling congress Agra, India, vol 3, pp 1551–1567
56. NTH (Norwegian Institute of Technology) (1988) Hard rock tunnel boring, Project report Trondheim, Norway, pp 1–86
57. Sapigni M, Berti M, Bethaz E, Busillo A, Cardone G (2002) TBM performance estimation using rock mass classifications. Int J Rock Mech Min Sci 39:771–788

T. Ramamurthy